Identification of the functional form of nonlinear effects of localized finite absorption in a diffusing medium

H. L. Graber[1], R. L. Barbour[1,2], J. Chang[2]
[1]Department of Physiology and Biophysics,
[2]Department of Pathology,
SUNY Health Science Center at Brooklyn
450 Clarkson Ave., Brooklyn, NY 11203

R. Aronson
Bioimaging Sciences Corp.
64 Burnett Terrace
W. Orange, NJ 07052

Abstract

A linear perturbation model for reconstructing images of absorption (Σ_a) and scattering (Σ_s) cross sections of a highly scattering medium is presented. Two factors limiting the accuracy of images reconstructed from linear perturbation models are described. These are the self–shadowing effect of a single perturbation and the mutual coupling effect of two perturbations. A relaxation method to numerically solve the diffusion equation for a slab geometry and to compute the flux of diffuse light crossing both surfaces of an initially nonabsorbing ($\Sigma_s = 1.0$, $\Sigma_a = 0.0$) slab, as the Σ_a in one or two cells of the medium is increased. When a single voxel was perturbed, it was found that: 1) for all voxel locations considered, a plot of change in light flux *vs.* change in Σ_a deviates significantly from a straight line when the additional Σ_a exceeds ~0.1; 2) the rate at which the flux perturbation approaches its limiting value as Σ_a increases is independent of the detector location; 3) with the exception of voxels in the immediate vicinity of the source, the rate at which the flux perturbation approaches its limiting value as Σ_a increases is independent of the location of the perturbed voxel. When two voxels were perturbed simultaneously, it was found that: 1) the distance separating two voxels is the most important determinant of the maximal mutual coupling effect they can have; 2) the maximal mutual coupling effect falls rapidly as the distance between two voxels increases; 3) if both perturbed voxels are lie in the same layer (*i.e.*, depth), the rate at which the mutual coupling effect approaches its limiting value as the Σ_a perturbations increase is independent of the detector location; 4) when the perturbed voxels are in different layers, there is a small but significant difference between the effects of mutual coupling on the diffuse transmission and on the diffuse reflectance. Low–order rational functions are sufficient for modeling both the self–shadowing and mutual coupling effects. Methods for modifying image reconstruction algorithms to incorporate corrections for these two effects are discussed.

1. Introduction

In several publications we have shown reconstructed images of random media whose scattering and absorption properties are similar to those of tissue illuminated by near infrared radiation, obtained by various algebraic techniques that solve a linear perturbation equation of the form $\Delta \boldsymbol{I} = \mathbf{W}\Delta\mathbf{x}$ (1)[1–5]. In this equation, $\Delta \boldsymbol{I}$ is the vector of changes, or perturbations, in detector readings with respect to some standard, or reference, medium; $\Delta\mathbf{x}$ is the vector of perturbations in some quantity such as Σ_a or Σ_s in the interior with respect to the same reference; and $\mathbf{W}$ is a matrix of weights relating the internal perturbations to those at the surface. Formulas for calculating elements of $\mathbf{W}$ for a particular problem have been derived from radiation transport theory[5,6]; the form of the weight function depends on the type of perturbation and the type of illumination/detection method used (*i.e.*, steady–state, time domain, or frequency domain; and whether absorption or emission (fluorescence, phosphorescence) is detected). Note that although in practice a reference medium chosen is frequently homogeneous, it is *not* necessary that it be so.

0-8194-1736-X/95/$6.00

Two premises underlying the mathematical model in (1) are: 1) that the change in light flux entering a given detector is directly proportional to the change in the optical cross sections in any voxel, and 2) that the net change in detected flux due to a change in two or more voxels is equal to the sum of the effects of each voxel considered separately. In fact, both premises become increasingly inaccurate as $\Delta\mathbf{x}$ increases. For example, if the Σ_a in one selected voxel increases by constant increments, the consequent reduction in detected light flux grows sublinearly, and eventually reaches a finite limiting value; additionally, the net reduction in detected light flux due to an increase in Σ_a in two voxels at once is smaller than the sum of the individual effects (see Figure 1). The practical effect of both phenomena is that solving (1) for $\Delta\mathbf{x}$ gives to an underestimate of the true internal perturbation in the medium.

Figure 1

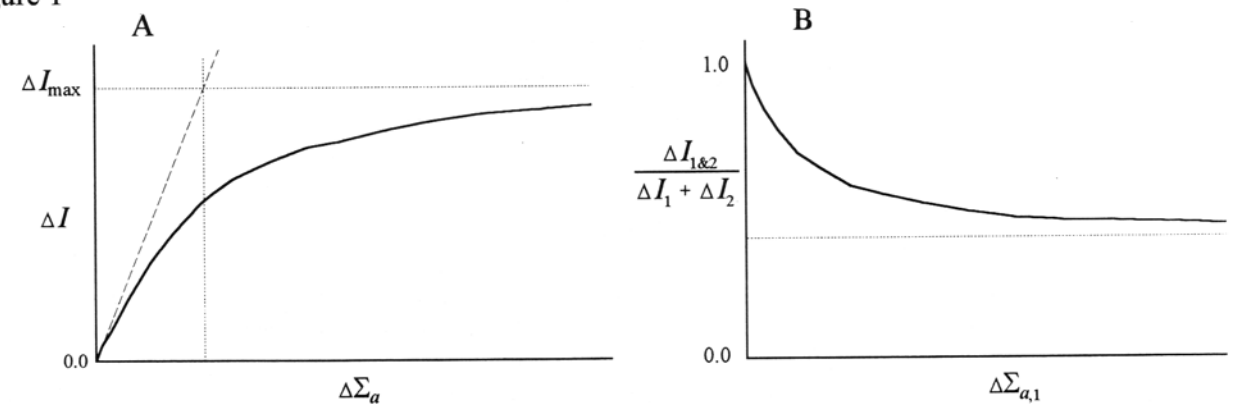

A) Hypothetical function (solid curve) relating increased absorption in a single voxel to the consequent change in light flux across a given point on the medium's surface. Dashed line is the linear relation expected according to (1). Horizontal dotted line is the maximum reduction in detector reading that can be produced by increasing the Σ_a in this voxel. Dotted vertical line shows the greatest value for $\Delta\Sigma_a$ that could be calculated by (1) for an absorber in this voxel.

B) Hypothetical function (solid curve) showing reduced effect of two voxels whose Σ_as are perturbed simultaneously compared to the sum of the individual effects of the two perturbations. Curve shown is a one–dimensional section through a two–dimensional surface; in this section the Σ_a is varied in one voxel while that in the other remains at a constant nonzero value.

The existence of these nonlinear effects, as well as higher–order ones involving coupling among more than two perturbations, is implicitly recognized in image recovery schemes in which $\Delta\mathbf{x}$ is calculated from (1) and then this solution is used to revise the elements of $\mathbf{W}$, which in turn gives rise to a revised $\Delta\mathbf{x}$[7,8]. The usual prescription is to continue this sequence of alternately updating $\mathbf{W}$ and $\Delta\mathbf{x}$ until the difference between successive estimates of $\Delta\mathbf{x}$ meets some preselected convergence criterion. Algorithms of this type are conditioned on a premise that the magnitude of the effects described above can be expected to be great enough that some sort of updating process will be necessary for reconstruction of accurate images. We are not aware, however, of any previously published report on direct measurements or computations of deviations from linear detector responses.

For the present study, we undertook to quantify these nonlinear relationships, using a homogeneous, nonabsorbing, slab medium as the reference, and a numerical method to compute solutions to a discretized version of the diffusion equation. The goals of these computations were to place some upper bound on the $\Delta\mathbf{x}$ that can be accurately obtained from (1) and to determine if corrections could be incorporated into a practical image reconstruction algorithm. Only the case of steady–state (cw) illumination and detection, and perturbations of only the absorption cross section were explicitly modeled in this first study. Theoretical calculations corroborating and expanding on the results shown below will be presented elsewhere[9]. Below, we present the results obtained from the one–voxel and two–voxel perturbation studies, show that excellent fits to the computed data sets are obtained from low–order rational functions, and show that the rates at which both types of curves

shown in Figure 1 approach their limiting value exhibit very little dependence on the location of the detector relative to the source and the perturbed voxels.

2. Methods

A previously described relaxation method[10] was used to compute the cw intensity of light in all cells of the model media and the flux of light at a total of 162 locations on two of the media's surfaces (see Figure 2). These two surfaces are designated "top" and "bottom"; the top surface is illuminated and the bottom surface is parallel to the top; 61 detectors were modeled on each of these surfaces. The reference medium for the computations was a nonabsorbing, homogeneous slab whose dimensions (length×width×thickness) were 61×61×11 cells, each of which represents the discrete spatial step a photon takes during each discrete time step. In each time step, all light in any one cell is distributed among its six nearest neighbors. In order to compute solutions to the isotropic (scalar) diffusion equation, the transmission probabilities in each cell are set so that the light in each cell is equally distributed among its six neighbors. Consequently, 5/6 of the light in each surface cell remains in the medium in each time step, and the remaining 1/6 escapes.

Figure 2

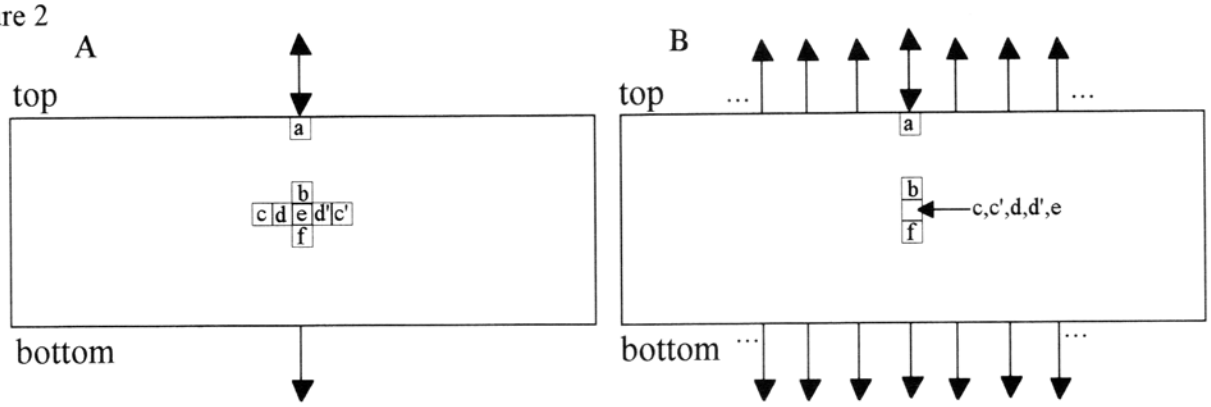

A) x–z section through medium modeled in the computations, in a plane containing the source (shown as arrow entering the slab). Dimensions of this section are 61 cells long × 11 cells thick. The cells that were perturbed are shown explicitly; cell a abuts the top surface (layer 1), cell b is in layer 5, cell f is in layer 7, all others are in layer 6. Detectors (shown as arrows exiting the slab) are in one–dimensional arrays perpendicular to this plane of section.

B) y–z section through medium modeled in the computations, in a plane containing the source (shown as arrow entering the slab). Dimensions of this section are 61 cells wide × 11 cells thick. Detectors (shown as arrows exiting the slab) arrays cover the entire width of the slab, 61 on each surface.

For the self–shadowing studies, the detector readings were first computed and stored for the reference medium case, in which the transport probability was equal to 1.0 in each cell (*i.e.*, absorption probability equal to 0.0). Then the transport probability was set to 0.0 in one of the voxels designated b–f in Figure 2, and the computation was repeated. By comparing the two sets of detector readings, the greatest possible reduction in detector reading, ΔI_{max}, could be calculated for every detector and every location of the absorber. (For an absorber in position a, $\Delta \boldsymbol{I}_{max} = \boldsymbol{I}_0$, the detector readings in the reference medium case.) Then computations were performed for absorbers at many intermediate strengths (transport probability between 0.5 and 1.0) at each of the locations a–f. Values of $\Delta I/\Delta I_{max}$ were then calculated for all detectors, absorber locations, and absorption strengths.

For the mutual coupling studies, additional computations were performed, in which a nonzero absorption probability was simultaneously assigned to either the cells d and d′ or the cells b and f. Figure 3 shows all combinations of absorption strength that were explicitly modeled in these studies. Simultaneous comparison of the detector readings obtained in the

reference medium case to those obtained when only cell b (d) was perturbed, only cell f (d′) was perturbed, and when both b and f (d and d′) were perturbed gives the following measure of the percent mutual coupling:

$$\chi = 100\left(1 - \frac{\Delta I_{m\&n}}{\Delta I_m + \Delta I_n}\right),$$

where m and n are the two perturbed cells. A value of $\chi = 0\%$ would be obtained if the effects of the two cells are completely independent. If the effect of one cell is to completely block the other from having any effect on the detector, and the two cells are symmetrically placed with respect to the source, as in the case of d and d′, then a value of $\chi = 50\%$ would result. A value of $\chi = 100\%$ would be obtained if the effects of the two cells were to completely cancel each other out, so that exactly the same I is measured in the case of the perturbed medium as for the reference medium.

Figure 3

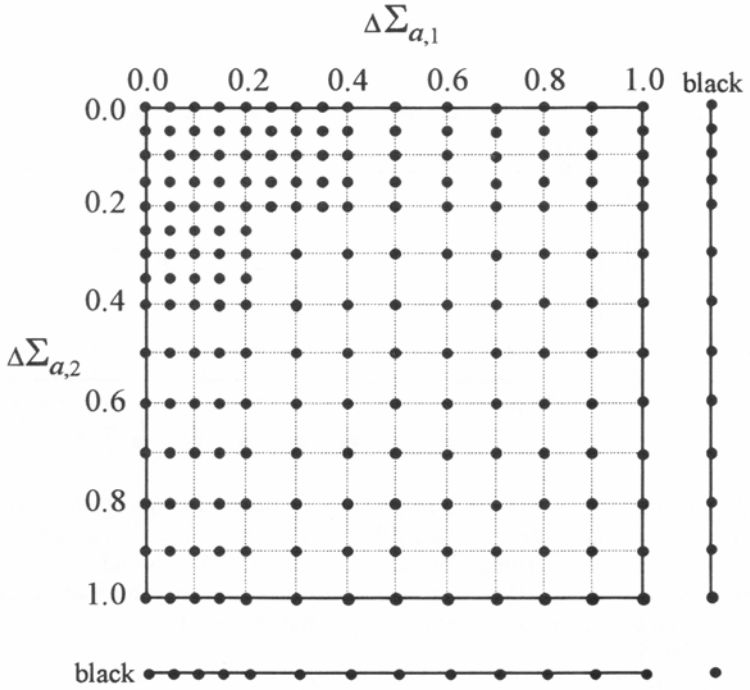

Black dots indicate pairs of absorption strengths that were explicitly modeled in at least one of the mutual coupling computations. When the absorption perturbation equals 1.0, the absorption and scattering cross sections in the cell are equal. In one case, the subscripts 1 and 2 denote cells d and d′, respectively; in the second case, the subscripts 1 and 2 denote cells b and f, respectively. In the former instance, because of the symmetric arrangement of the cells, only permutations for which $\Delta\Sigma_{a,1} \geq \Delta\Sigma_{a,2}$ were explicitly computed.

Additional computations were performed with perfect absorbers located simultaneously in the pairs of cells designated b and c, b and d, b and e, c and d, c and e, c and d′, c and c′, c and f, d and e, d and f, or e and f. The detector readings obtained from these computations and those previously described were used to calculate the dependence of the greatest attainable mutual coupling on the distance separating two cells, their orientation relative to the source, and their distance from the top surface.

3. Results

3.1 Computed detector responses

The detector responses across the "top" and "bottom" surfaces of the reference medium, and an example of the impact of a black absorber filling one cell, are shown in Figure 4. In a slab of truly infinite extent, the plot of $\log I_0$ would be expected to approach a straight line as the detector moves farther from the source; in this case, the curves do become nearly linear except

for the detectors within three steps of the ends of the slab (Figure 4A). The rate at which the two curves approach their common asymptotes would be expected to increase with slab thickness. When a black absorber is introduced in cell e (see Figure 2), there is an appreciable reduction in detected light at all locations except those in the immediate vicinity of the source (Figure 4B). This is the percentage of light detected in the reference medium case that traversed the affected cell at least once. The same limiting value for the absorption effect is attained on both surfaces, and the edge effect appears to cancel out entirely in the calculation of the ratio of ΔI to I_0.

Figure 4

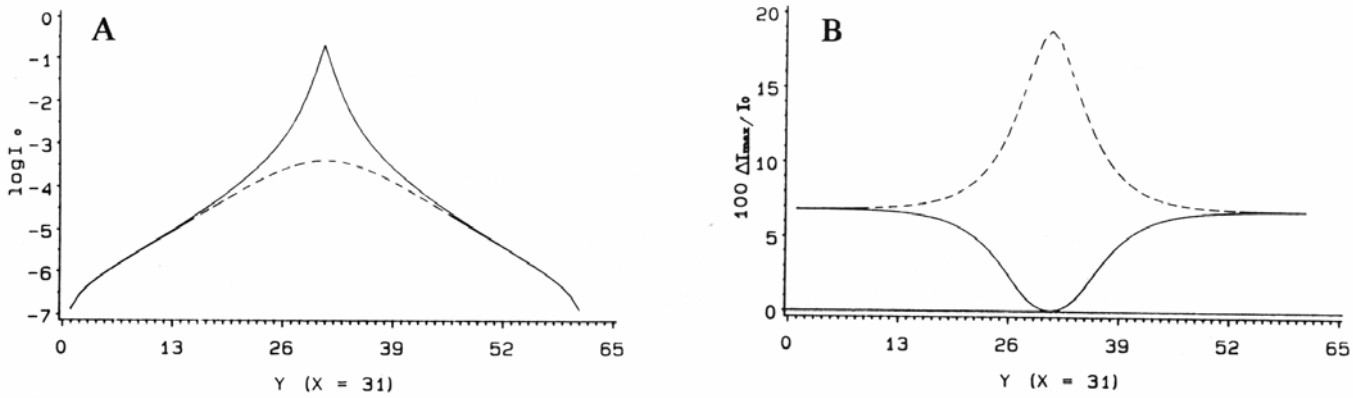

A) Intensity of detected light on top (Z = 1, solid curve) and bottom (Z = 11, dashed curve) surfaces of the homogeneous reference medium. cw light of unit intensity enters slab at position X = 31, Y = 31 of top surface. Quantity plotted is the common log of the detector reading at every position in the detector arrays (see Figure 2). B) % reduction in detector readings, $\Delta I / I_0$, when a black absorber is placed in cell e. Solid curve = impact on detectors on top surface; dashed curve = impact on detectors on bottom surface.

3.2 Self–shadowing *vs.* absorption

After I was computed for an absorber in cell e and $\Delta\Sigma_a = 0.01, 0.02, ..., 0.10, 0.15, ..., 0.4, 0.5, ..., 1.0$, plots of ΔI *vs.* $\Delta\Sigma_a$ for various detectors yielded curves similar to that sketched in Figure 1A. From these, it was apparent that (1) is an adequate approximation when $\Delta\Sigma_a \leq 0.10$ (see Figure 5A). Due to the large range of source–detector separations modeled, there was considerable variation in the absolute values of ΔI_{max} for different detectors. We chose to replot the data as $\Delta I/\Delta I_{max}$ *vs.* $\Delta\Sigma_a$, as the ratio would always lie in the range 0 – 1. Curves for several detectors then could be plotted simultaneously, for study of the relative rates at which ΔI approaches ΔI_{max} at different locations. When this was done (Figure 5A), it was discovered that essentially the same function was obtained for all detectors on both surfaces, with the small differences among them easily attributable to the finite precision of the relaxation computations.

Because we had not yet deduced the form of the function shown in Figure 5A from transport theory[9], attempts were made to fit the computed points to rational function models. The simplest such model is a rectangular hyperbola, *i.e.*,

$$\frac{\Delta I}{\Delta I_{max}} = \frac{\Delta\Sigma_a}{\Delta\Sigma_a + k}. \qquad (2)$$

A prediction of this model is that if the data points are replotted as $\Delta\Sigma_a\Delta I_{max}/\Delta I$ *vs.* $\Delta\Sigma_a$,, they should fall on straight lines. When the indicated replots were made (Figure 5B), the predicted behavior was seen, with very little variation in the slopes or intercepts of the regression lines. A nonlinear regression routine was then used to fit the data directly to the model in (2); when this was done, the coefficient of variation (COV) of the set of ks for all detectors was ~0.02% (mean value = 0.6844, standard deviation = 0.0002, range = 0.6842–0.6856; the absolute value of k is highly medium–specific).

Figure 5

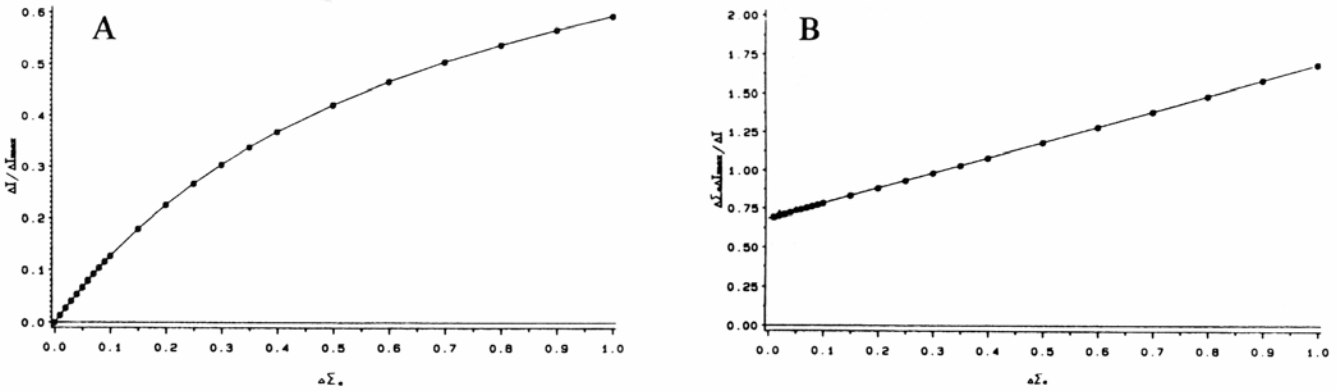

A) $\Delta I/\Delta I_{max}$ *vs.* $\Delta\Sigma_a$, *i.e.*, effect of finite absorber in cell e, relative to that of a black absorber. Plot contains four curves, for the detectors coincident with and directly opposite the source, and for the detectors farthest from the source on both the top and bottom surfaces. The differences among the four sets of points is smaller than the thickness of the interpolating curves. B) A replot of the data from A, with regression lines; the observation that the points lie on a straight line in this replot indicates that the rational function model in (2) gives an excellent fit to the data.

Analogous calculations were carried out on data for absorption in each of the other cells specified in Figure 2. The results are summarized in Figure 6. Plotted in Figure 6, Panel A are the mean value of $\Delta I/\Delta I_{max}$ for the entire set of detectors (left–hand vertical scale) and the COV (right–hand vertical scale), *vs.* $\Delta\Sigma_a$, when cell b is perturbed. The COV is < 0.1% for all values of $\Delta\Sigma_a$. Plotted in Figure 6, Panel B are the mean values of $\Delta I/\Delta I_{max}$ *vs.* $\Delta\Sigma_a$ for all six distinct absorber locations. It is seen that (2) is an appropriate model in all cases. The mean value of k is nearly the same for five of the six cells, the one exception being cell a, which lies immediately beneath the source.

Figure 6

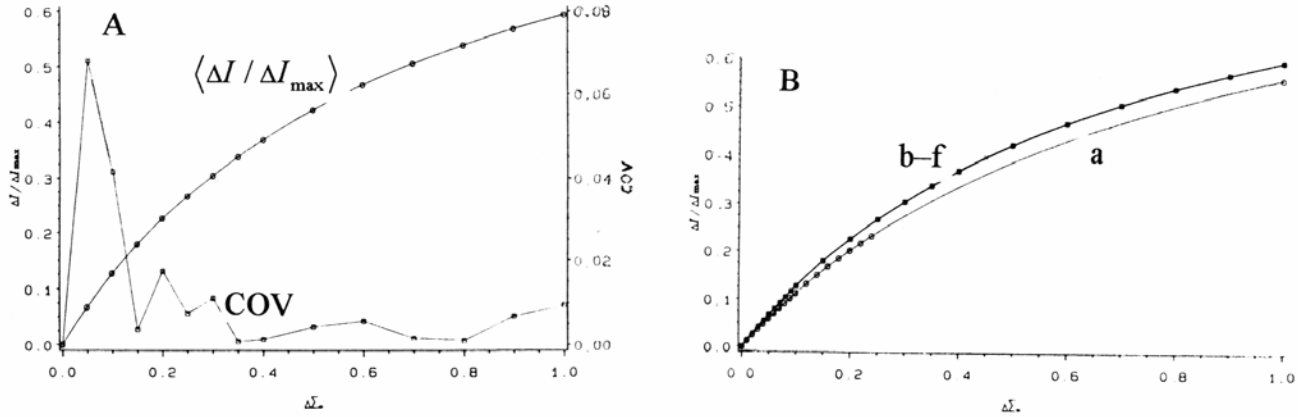

A) Mean value of $\Delta I/\Delta I_{max}$, and COV, as a function of $\Delta\Sigma_a$ in cell b. B) Mean values of $\Delta I/\Delta I_{max}$ as a function of $\Delta\Sigma_a$ in each of cells a–f. Five of the six curves obtained are nearly identical; the exception is that for cell a (circle symbols). Curves drawn through $\Delta I/\Delta I_{max}$ values in both A and B are fits of the model (2) to the data points. Adjacent COV points in A are joined by straight line segments.

3.3 Mutual coupling *vs.* absorption

After I was computed for an absorbers in cells d and d′, for all the ordered pairs of $(\Delta\Sigma_{a,\mathrm{d}}, \Delta\Sigma_{a,\mathrm{d}'})$ specified in Figure 3, the quantity $\xi \equiv \Delta I_{\mathrm{d\&d}'}/(\Delta I_{\mathrm{d}} + \Delta I_{\mathrm{d}'}) = \Delta I_{\mathrm{d\&d}'}/(2\Delta I_{\mathrm{d}})$ was plotted *vs.* $\Delta\Sigma_{a,\mathrm{d}}$ *vs.* $\Delta\Sigma_{a,\mathrm{d}'}$ for various detectors. Examples of one–dimensional sections through these surfaces, for the same four detectors as in Figure 5 and $\Delta\Sigma_{a,\mathrm{d}} = \Delta\Sigma_{a,\mathrm{d}'}$, are shown in Figure 7, Panel A. The plotted curves are qualitatively similar to that sketched in Figure 1B, and, with the exception of small deviations caused by the finite precision of the computations, at any given $(\Delta\Sigma_{a,\mathrm{d}}, \Delta\Sigma_{a,\mathrm{d}'})$ the same calculated value for ξ is calculated for all detectors on both surfaces. We supposed these curves to be hyperbolas, and attempted to fit ξ with a rational function of the form

$$\xi = \frac{k_1\Delta\Sigma_a + k_2}{\Delta\Sigma_a + k_2}, \qquad 0 < k_1 \leq 1, \qquad (3)$$
$$\Delta\Sigma_a = \Delta\Sigma_{a,\mathrm{d}} = \Delta\Sigma_{a,\mathrm{d}'}.$$

A prediction of this model is that if the data points are replotted as $\Delta\Sigma_a/(1 - \xi) = \Delta\Sigma_a(\Delta I_{\mathrm{d}} + \Delta I_{\mathrm{d}'})/[(\Delta I_{\mathrm{d}} + \Delta I_{\mathrm{d}'}) - \Delta I_{\mathrm{d\&d}'}]$ *vs.* $\Delta\Sigma_a$, they should fall on straight lines. When the indicated replots were made (Panel B), the predicted behavior was seen, with very little variation in the slopes or intercepts of the regression lines, although small errors in the original data are greatly amplified in this form of replot. A nonlinear regression routine was then used to fit the data directly to the model in (3); when this was done, the COV of the set of k_1s for all detectors was ~0.02% (mean value = 0.8780, standard deviation = 0.0001, range = 0.8776–0.8787) and the COV of the set of k_2s for all detectors was ~0.29% (mean value = 0.6010, standard deviation = 0.0017, range = 0.5913–0.6046).

Figure 7

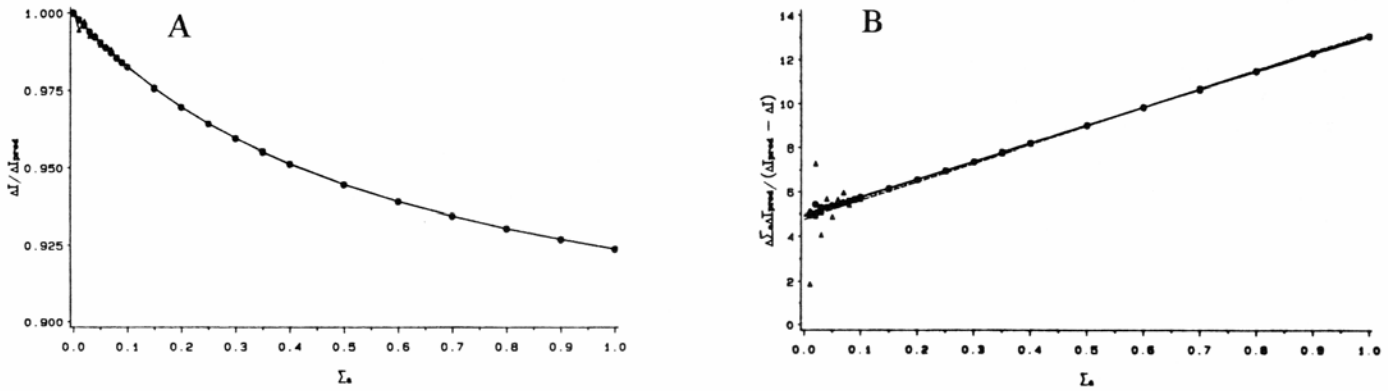

Mutual coupling effect of two absorbers in cells d and d′. According to (1), the predicted value of ΔI, ΔI_{pred}, when both cells are perturbed at once is just $\Delta I_{\mathrm{d}} + \Delta I_{\mathrm{d}'}$. A) Calculated values of $\xi \equiv \Delta I_{\mathrm{pred}}/(\Delta I_{\mathrm{d}} + \Delta I_{\mathrm{d}'})$ *vs.* $\Delta\Sigma_{a,\mathrm{d}}$, for the special case of $\Delta\Sigma_{a,\mathrm{d}} = \Delta\Sigma_{a,\mathrm{d}'}$; the ratio is ≤ 1, meaning (1) will underestimate the absorption strength. The rate at which ξ decreases with increasing $\Delta\Sigma_{a,\mathrm{d}}$ is almost exactly the same for all detectors. B) A replot of the data from A, with regression lines; the observation that the points lie on straight lines in this replot indicates that the rational function model in (3) gives an excellent fit to the data. The large deviations seen for one detector at small $\Delta\Sigma_{a,\mathrm{d}}$ values is an amplification of small errors, caused by the finite precision of the computations, in the original data. The detector exhibiting these errors is the one lying closest to the source, which has the smallest associated ΔI.

As was the case with self–shadowing, the general form of the function $\xi(\Delta\Sigma_{a,m},\Delta\Sigma_{a,n})$, where m and n may be any two cells, had not yet been deduced. Therefore, we continued to empirically fit the computed data with rational functions, and supposed that a model with the same form as (3) was correct for any constant–$\Delta\Sigma_{a,m}$ section or any constant–$\Delta\Sigma_{a,n}$ section through a $\xi(\Delta\Sigma_{a,m},\Delta\Sigma_{a,n})$ surface. Then it should be possible to fit the entire surface to a three–parameter model of the form:

$$\xi\left(\Delta\Sigma_{a,m},\Delta\Sigma_{a,n}\right)=\frac{k_m\Delta\Sigma_{a,m}+k_n\Delta\Sigma_{a,n}+k'_{m,n}\Delta\Sigma_{a,m}\Delta\Sigma_{a,n}}{k_m\Delta\Sigma_{a,m}+k_n\Delta\Sigma_{a,n}+\Delta\Sigma_{a,m}\Delta\Sigma_{a,n}},$$

which has the necessary property that $\xi = 1$ when either $\Delta\Sigma_{a,m} = 0$ or $\Delta\Sigma_{a,n} = 0$. It was also decided that a previously described quantity, χ, provided a more intuitive measure than ξ of mutual coupling; the two are related by $\chi = 100(1 - \xi)$. The proposed model function for $\chi(\Delta\Sigma_{a,m},\Delta\Sigma_{a,n})$ is

$$\chi\left(\Delta\Sigma_{a,m},\Delta\Sigma_{a,n}\right)=\frac{100\cdot k_{m,n}\Delta\Sigma_{a,m}\Delta\Sigma_{a,n}}{k_m\Delta\Sigma_{a,m}+k_n\Delta\Sigma_{a,n}+\Delta\Sigma_{a,m}\Delta\Sigma_{a,n}}, \tag{4}$$

where $k_{m,n} = 1 - k'_{m,n}$.

The mean values, over the entire set of detectors, of $\chi(\Delta\Sigma_{a,d},\Delta\Sigma_{a,d'})$ and $\chi(\Delta\Sigma_{a,b},\Delta\Sigma_{a,f})$ were calculated directly from the computed detector readings. The resulting surfaces are plotted in Figure 8, Panels A and B. The former surface is, by necessity, symmetric about $\Delta\Sigma_{a,d} = \Delta\Sigma_{a,d'}$, while the latter has, as expected, a pronounced asymmetry. However, the difference between the surfaces becomes very small when there is strong absorption in both cells. In the limiting case of a black absorber in both cells, the maximum mutual coupling, χ_{max}, is between 12% and 13% for both media, suggesting the distance between the cells is the primary determinant of χ_{max}, and their orientation relative to the surfaces and source is of secondary importance.

A nonlinear regression routine was then used to fit the data directly to the model in (4). The parameter values determined for $\chi(\Delta\Sigma_{a,d},\Delta\Sigma_{a,d'})$ are: $k_d = k_{d'} = 0.3045 \pm 0.0009$, $k_{d,d'} = 0.1221 \pm 0.0002$; for $\chi(\Delta\Sigma_{a,b},\Delta\Sigma_{a,f})$, they are: $k_b = 0.434 \pm 0.001$, $k_f = 0.1830 \pm 0.0008$, $k_{b,f} = 0.1236 \pm 0.0002$. The relative percent error, $100(\chi_{data} - \chi_{model})/\chi_{data}$, in these fits are plotted in Figure 8, Panels C and D. It is seen that the absolute value of this error is always < 0.1%.

When calculated values of $\chi(\Delta\Sigma_{a,d},\Delta\Sigma_{a,d'})$ and $\chi(\Delta\Sigma_{a,b},\Delta\Sigma_{a,f})$ for individual detectors were compared (data not shown), almost no variability was found among the different detectors in the former case, and a small but significant degree of variability in the latter case. When cells d and d′ were perturbed, the COV was always < 0.1%, but when strong absorbers were placed in both b and f, COV values ≥ 1% were obtained. More significant than the absolute magnitude of the COV in this case is the observation that it systematically increases as the absorption perturbation in one or both cells increases (see following section, and Discussion).

Figure 8

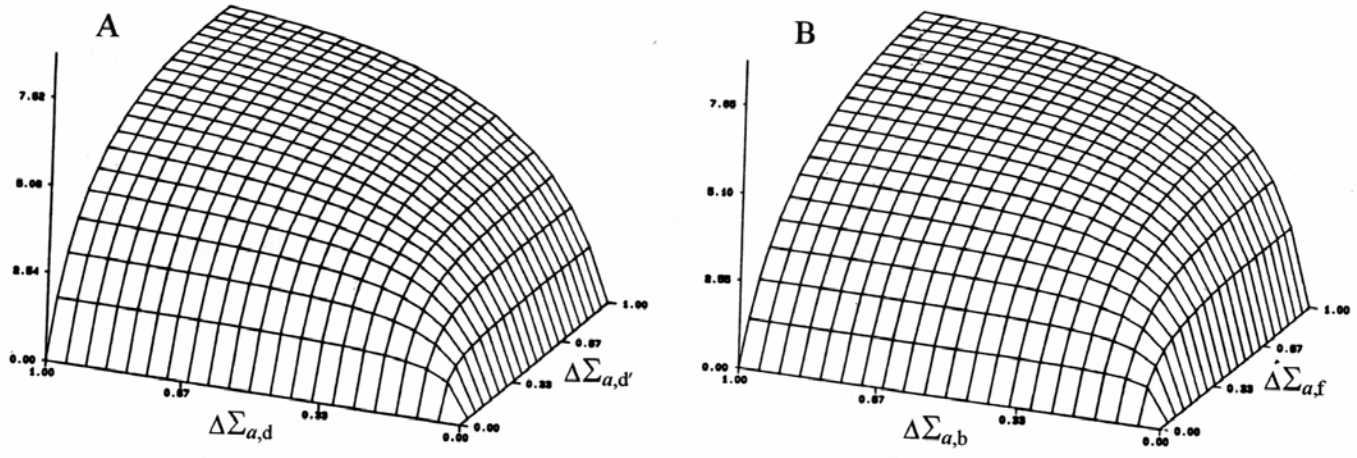

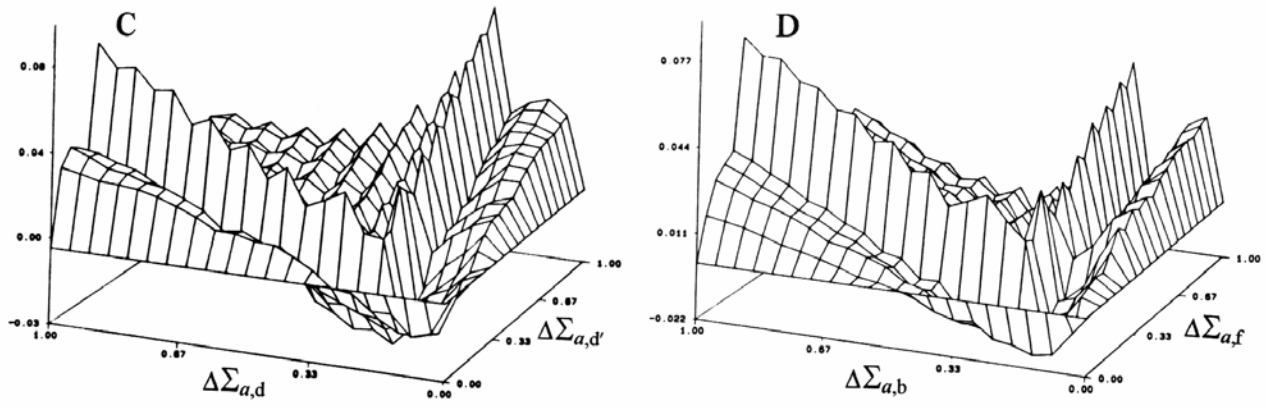

Surface plots of mutual couplings calculated from computed ΔIs. A) $\chi(\Delta\Sigma_{a,\mathrm{d}},\Delta\Sigma_{a,\mathrm{d}'})$ *vs.* $\Delta\Sigma_{a,\mathrm{d}}$ *vs.* $\Delta\Sigma_{a,\mathrm{d}'}$; because of the symmetry of cells d and d′, $\Delta I_{\mathrm{d},\mathrm{d}'}$ was explicitly computed only for $\Delta\Sigma_{a,\mathrm{d}} \geq \Delta\Sigma_{a,\mathrm{d}'}$. B) $\chi(\Delta\Sigma_{a,\mathrm{b}},\Delta\Sigma_{a,\mathrm{f}})$ *vs.* $\Delta\Sigma_{a,\mathrm{b}}$ *vs.* $\Delta\Sigma_{a,\mathrm{f}}$. C) Relative percent error between calculated $\chi(\Delta\Sigma_{a,\mathrm{d}},\Delta\Sigma_{a,\mathrm{d}'})$ values and the best–fitting model of the form in (4). D) Relative percent error between calculated $\chi(\Delta\Sigma_{a,\mathrm{b}},\Delta\Sigma_{a,\mathrm{f}})$ values and the best–fitting model of the form in (4).

3.4 Maximum mutual coupling *vs.* distance

As explained above (see Methods), detector readings were computed with a single black absorber in each of the positions b–f shown in Figure 2, and with two black absorbers in each of the thirteen pairs of cells specified in Table 1. If χ were zero for all cell pairs, then due to the symmetry of cells d and d′ (c and c′) with respect to the detectors, the net ΔI at any detector due to absorbers in both d and d′ (c and c′) would be exactly twice that due to an absorber in d (c) alone. Similarly, the net ΔI due to absorbers in c and d simultaneously would be exactly the same as that due to absorbers in c and d′ simultaneously.

The average value of $\chi_{\max}$ taken over all 62 distinct detectors on both the top and bottom surfaces of the slab are shown in Table 1. It is seen that the inter–cell separation is the most important determinant of the mean value of the maximum attainable mutual coupling, with the depth of the cells and their orientation with respect to the surfaces having a much smaller impact. However, only in those cases in which both perturbed cells are in the same layer are the standard

Table 1: maximum attainable % mutual coupling, χ, averaged over all detectors

cells	separation[a]	mean	s. d.	range
b, e	1[b]	24.20	1.9	20.95 – 26.95
c, d	1	23.87	0.10	23.58 – 23.96
d, e	1	23.98	0.016	23.92 – 23.99
e, f	1	23.82	0.98	21.55 – 26.95
b, d	$\sqrt{2}$[c]	15.94	0.69	13.75 – 17.48
d, f	$\sqrt{2}$	15.86	0.48	14.81 – 17.48
b, f	2	12.27	1.59	8.49 – 17.20
d, d′	2	12.20	0.0087	12.13 – 12.20
c, e	2	12.11	0.079	11.90 – 12.17
b, c	$\sqrt{5}$	9.81	0.51	8.02 – 10.56
c, f	$\sqrt{5}$	9.97	0.16	9.76 – 10.56
c, d′	3	7.10	0.023	7.05 – 7.12
c, c′	4	4.59	0.012	4.58 – 4.68

Average value of χ over the 62 distinct detectors on the top and bottom surfaces, standard deviation, minimum and maximum values in the range. For most cell pairs, the minimum value belongs to the detector coinciding with the source and the maximum value to the detector directly in line with the source. *a*: separation is the distance between the centers of the cell pairs, so two cells with a face in common have a separation of 1; *b*: cell pairs with this separation have a common face; *c*: cell pairs with this separation have a common edge.

deviation and range sufficiently small to support a conclusion that the coefficients in (3) are independent of the detector location. In the other cases, χ_{max} varies over an appreciable range among different detectors.

Due to the locations of the cells that are perturbed, two explanations for some the large ranges seen in some cases are possible. The most important factor could be the different depths of the two absorbers, or it could be the fact that in every such case at least one of the perturbed cells lies directly in line with the source. The former possibility seems more attractive, because the range is very small in two cases (c and e, d and e) in which one cell lies directly in line with the source but both are in the same layer. As a further test, for every pair containing at least one cell in line with the source, the mean value of χ_{max}, its standard deviation, and the range were calculated separately for detectors of backscattered and of transmitted light. The results are presented in Table 2. It is seen that when both cells are in the same layer, the mean values are the same on both surfaces, and the ranges are almost identical. However, when they are in different layers, there is a small but significant difference between the backscatter mean and the transmission mean, and the ranges either barely overlap or are completely disjoint.

Table 2: maximum attainable % mutual coupling, χ, averaged over top and bottom surfaces separately, when at least one perturbed cell is directly in line with the source

cells	separation	surface	mean	s. d.	range
b, e	1	top	23.59	0.98	20.95 – 24.23
		bottom	24.81	0.83	24.24 – 26.95
d, e	1[a]	top	23.98	0.018	23.92 – 23.99
		bottom	23.98	0.015	23.94 – 23.99
e, f	1	top	23.28	0.69	21.55 – 23.76
		bottom	24.36	0.94	23.76 – 26.95
b, d	$\sqrt{2}$	top	15.56	0.68	13.75 – 16.01
		bottom	16.32	0.45	16.02 – 17.48
d, f	$\sqrt{2}$	top	15.60	0.29	14.81 – 15.79
		bottom	16.12	0.49	15.79 – 17.48
b, f	2	top	11.39	1.15	8.49 – 12.18
		bottom	13.15	1.49	12.19 – 17.20
c, e	2[a]	top	12.11	0.080	11.90 – 12.17
		bottom	12.11	0.079	11.91 – 12.17
b, c	$\sqrt{5}$	top	9.54	0.60	8.02 – 9.97
		bottom	10.08	0.19	9.96 – 10.56
c, f	$\sqrt{5}$	top	9.89	0.047	9.76 – 9.92
		bottom	10.04	0.19	9.91 – 10.56

Mean value of χ_{max}, standard deviation, and range, for detectors on top surface (backscatter) and on bottom surface (transmission). When the perturbed cells are in different layers, the two partial ranges either don't overlap at all or overlap only slightly. *a*: the two cells in this case are in the same layer.

A smaller disparity than that just described could be expected, however, if the perturbed cells were moved to a location more distant from the source. The largest range for χ_{max} occurs when the perturbed cells are b and f, both of which are directly in line with the source, and the only pair separated by two layers. The minimum value for χ_{max}, 8.49%, belongs to the detector coinciding with the source. The maximum value, 17.20%, belongs to the detector directly in line with the source. It is to be expected that if the separation between these two absorbers were to increase, with one approaching the source and the other approaching the in–line detector, the maximum χ_{max} would rapidly rise to 50% and the minimum would fall nearly to 0%. Clearly, if the cells were not in line with the source, the difference between the greatest and least χ_{max}s would be smaller.

Finally, note that the absorption perturbations in target media of interest are expected to be smaller than those used for this portion of the present study. The rate at which the maximum attainable χ falls with increasing separation suggests that in practice, explicit corrections for mutual coupling will not be necessary for volume elements separated by more than ~2 transport mean free pathlengths.

4. Discussion

If (2) is the correct form for the effect of a single localized absorption perturbation on the ratio $\Delta I/\Delta I_{max}$, then we can derive an equation that is analogous to (1), but that takes into account the self–shadowing effect of absorbers. For a given set of source, detector, and voxel locations, we have

$$\Delta I = \frac{\Delta I_{max} \Delta \Sigma_a}{\Delta \Sigma_a + k}.$$

In the limit of very small $\Delta\Sigma_a$, this becomes

$$\Delta I \xrightarrow{\Delta\Sigma_a \to 0} \left(\frac{\Delta I_{max}}{k} \right) \Delta \Sigma_a .$$

But, from (1), it is also true that

$$\Delta I \xrightarrow{\Delta\Sigma_a \to 0} w \Delta \Sigma_a ,$$

where specific formulas for w have been derived from transport theory[6]. Therefore, we have $k = \Delta I_{max}/w$, and

$$\Delta I = \frac{w \Delta I_{max} \Delta \Sigma_a}{w \Delta \Sigma_a + \Delta I_{max}}.$$

Note that ΔI, w, and ΔI_{max} are functions of the source, detector, and voxel locations. On the other hand, the ratio $\Delta I_{max}/w$ is certainly independent of detector location for a given source and voxel. It also appears to be, except in the immediate vicinity of a source, independent of the voxel location (although an insufficient number of different voxel locations had been explicitly examined at the time of this writing to be certain); if this is true, then its dependence on the source location would also be very weak, as translating an absorber in one direction at a fixed depth is equivalent to translating the source in the opposite direction. Once the value of a given voxel's ΔI_{max} is known for any one detector, the relation $\Delta I_{max,2} = (w_2/w_1)\, \Delta I_{max,1}$ can be used to calculate ΔI_{max} for all the other detectors. If the voxel in question is at the surface, there is a straightforward solution to the problem of finding the first ΔI_{max} value. A detector can be placed directly over the voxel and, for that detector, $\Delta I_{max} = I_0$. To the extent that the ratio $\Delta I_{max}/w$ is independent of the voxel location, estimates of ΔI_{max} could then be readily obtained for all voxels and all detectors.

The hypothesis of independence of $\Delta I_{max}/w$ on detector location was explicitly tested, using weights and detector readings computed by Monte Carlo simulations of photon migration in a cylindrical medium[6]. As shown in Figure 9, Panel A, because the perturbed voxel is immediately adjacent to the source, $\Delta I_{max} = I_0$ for all detectors. When $\log w$ *vs.* θ and $\log I_0$ *vs.* θ are plotted, the curves are seen to be nearly parallel (Panel B). This is confirmed when the data are replotted as $\log w$ *vs.* $\log I_0$ (Panel C).

Suppose ΔI_{max} is known for all sources, detectors, and voxels. Corresponding to source j and detector k, we have an equation of the form:

$$\begin{aligned} \Delta I_{jk} &= \sum_i \frac{\Delta I_{ijk}^{max} w_{ijk} \Delta \Sigma_{a,i}}{w_{ijk} \Delta \Sigma_{a,i} + \Delta I_{ijk}^{max}} \\ &= \sum_i \left(\frac{\Delta I_{ijk}^{max} w_{ijk}}{w_{ijk} \Delta \Sigma_{a,i} + \Delta I_{ijk}^{max}} \right) \Delta \Sigma_{a,i} \\ &= \sum_i w'_{ijk} \Delta \Sigma_{a,i} . \end{aligned}$$

That is, a set of detector readings gives rise to a system of *non*linear equations. This could be converted to a linear system if we knew all the values for w'_{ijk}. However, in order to calculate w'_{ijk}, we have first to know $\Delta\Sigma_{a,i}$, which is the unknown. The following iterative process should converge to the correct $\Delta\Sigma_{a,i}$:

1) Let $\Delta I_{jk} = \sum_i w^0_{ijk}\Delta\Sigma^0_{a,i}$, where w^0_{ijk} is the weight in (1). Solve linear system for all $\Delta\Sigma^0_{a,i}$.

2) Calculate $w^1_{ijk} = \dfrac{\Delta I^{\max}_{ijk} w^0_{ijk}}{w^0_{ijk}\Delta\Sigma^0_{a,i} + \Delta I^{\max}_{ijk}}$ for all i, j, k.

3) Let $\Delta I_{jk} = \sum_i w^1_{ijk}\Delta\Sigma^1_{a,i}$. Solve linear system for all $\Delta\Sigma^1_{a,i}$.

4) Calculate $w^2_{ijk} = \dfrac{\Delta I^{\max}_{ijk} w^0_{ijk}}{w^0_{ijk}\Delta\Sigma^1_{a,i} + \Delta I^{\max}_{ijk}}$ for all i, j, k.

This sequence of alternately calculating revised w^n_{ijk} s and $\Delta\Sigma^n_{a,i}$ s is repeated until the difference between successive estimates of $\Delta\Sigma_{a,i}$ falls below a preset threshold.

Figure 9

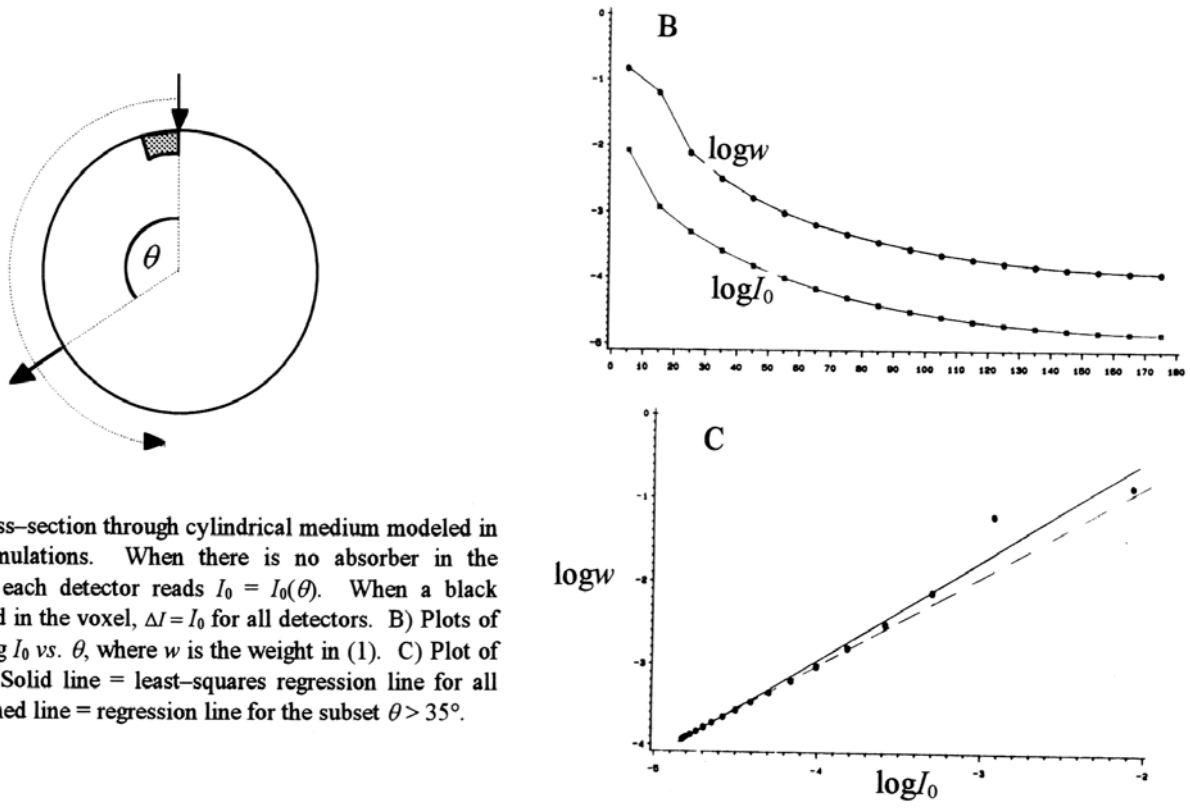

A) Sketch of cross–section through cylindrical medium modeled in Monte Carlo simulations. When there is no absorber in the indicated voxel, each detector reads $I_0 = I_0(\theta)$. When a black absorber is placed in the voxel, $\Delta I = I_0$ for all detectors. B) Plots of log$w$ *vs.* θ and log I_0 *vs.* θ, where w is the weight in (1). C) Plot of log$w$ *vs.* log I_0. Solid line = least–squares regression line for all data points. Dashed line = regression line for the subset $\theta > 35°$.

Taking both the individual and pairwise effects of absorbers into account, the nonlinear equation corresponding to each source–detector combination is

$$\Delta I_{jk} = \frac{1}{N-1}\sum_i\sum_{i'>i}\left(\frac{\Delta I^{\max}_{ijk} w_{ijk}\Delta\Sigma_{a,i}}{w_{ijk}\Delta\Sigma_{a,i} + \Delta I^{\max}_{ijk}} + \frac{\Delta I^{\max}_{i'jk} w_{i'jk}\Delta\Sigma_{a,i'}}{w_{i'jk}\Delta\Sigma_{a,i'} + \Delta I^{\max}_{i'jk}}\right)\left(\frac{\alpha_{ii'jk}\Delta\Sigma_{a,i} + \beta_{ii'jk}\Delta\Sigma_{a,i'} + \gamma_{ii'jk}\Delta\Sigma_{a,i}\Delta\Sigma_{a,i'}}{\alpha_{ii'jk}\Delta\Sigma_{a,i} + \beta_{ii'jk}\Delta\Sigma_{a,i'} + \Delta\Sigma_{a,i}\Delta\Sigma_{a,i'}}\right),$$

where N is the number of voxels in the target. An iterative algorithm of the type just described can be modified to incorporate the additional term. However, before the result can be applied in practice, estimates of the coefficients α, β, and γ would be needed for each source, detector, and *pair* of voxels. The results presented here indicate that there is, in general, no simple way of deducing the coefficients for one combination from those of others. Some findings, such as the independence of mutual coupling on detector position when the two cells are in the *same layer*, are encouraging.

The results of the mutual coupling studies would suggest, however, that for most source, detector, and voxel pair combinations, its effect is quite small. The average value of χ, ~7.5%, when $\Delta\Sigma_a$ was 0.5 in both cells b and f or d and d′ is certainly significant, but perturbations of such magnitude (*i.e.*, $\Delta\Sigma_a = \Sigma_s/2$) are much larger than those we expect to encounter in practical problems of clinical interest. Note that $\chi < 2\%$ when $\Delta\Sigma_a < 0.1$ in both cells. From these findings, we can conclude that a mutual coupling correction need not consider pairs of voxels separated by more than ~2 transport mfp.

5. Acknowledgment

This work was supported, in part, by NIH grant R01 CA59955, by the New York State Science and Technology Foundation, and by ONR grant N000149510063.

6. References

[1] R. L. Barbour, H. L. Graber, Y. Wang, J. Chang, R. Aronson, "A perturbation approach for optical diffusion tomography using continuous–wave and time–resolved data," *Medical Optical Tomography: Functional Imaging and Monitoring*, SPIE Institutes vol. IS11, pp. 87–120, 1993.

[2] H. L. Graber, J. Chang, R. Aronson, R. L. Barbour, "A perturbation model for imaging in dense scattering media: derivation and evaluation of imaging operators," *Medical Optical Tomography: Functional Imaging and Monitoring*, SPIE Institutes vol. IS11, pp. 121–143, 1993.

[3] J. Chang, H. L. Graber, R. L. Barbour, "Image reconstruction of targets in random media from CW laser measurements and simulated data," *Advances in Optical Imaging and Photon Migration*, Optical Society of America, vol. 21, pp. 193–201, 1994.

[4] W. Zhu, Y. Wang, H. L. Graber, R. L. Barbour, J. Chang, "A regularized progressive expansion algorithm for recovery of scattering media form time–resolved data," *Advances in Optical Imaging and Photon Migration*, Optical Society of America, vol. 21, pp. 211–216, 1994.

[5] J. Chang, H. L. Graber, R. L. Barbour, "Progress toward optical mammography: imaging in dense scattering media using time–independent optical sources," *Proc. 1994 IEEE Medical Imaging Conference (Norfolk, VA)*, Nov. 1994, (in press).

[6] J. Chang, H. L. Graber, R. L. Barbour, "Imaging diffusive media using time–independent and time–harmonic sources: dependence of image quality on imaging algorithms, target volume, weight matrix, and view angles," accompanying paper in these proceedings.

[7] S. R. Arridge, "The forward and inverse problems in time resolved infra–red imaging," *Medical Optical Tomography: Functional Imaging and Monitoring*, SPIE Institutes vol. IS11, pp. 35–64, 1993.

[8] B. W. Pogue, M. S. Patterson, "Forward and inverse calculations for near–infrared imaging using a multigrid finite difference method," *Advances in Optical Imaging and Photon Migration*, Optical Society of America, vol. 21, pp. 176–180, 1994.

[9] Manuscript in preparation.

[10] F. H. Schlereth, J. M. Fossaceca, A. D. Keckler, R. L. Barbour, "Imaging in diffusing media with a neural net formulation: a problem in large scale computation," *Proc. Physiological Monitoring and Early Detection Diagnostic Methods*, SPIE vol. 1641, pp. 46–57, 1992.